한국마린엔지니어링학회지 제31권, 제2호, pp. 190~196, 2007. 3 (ISSN 1226-9549)
Journal of the Korean Society of Marine Engineering

3D Finite Element Analysis of Contact-less Power Supply with Linear Servo Motor

Kyung-il Woo† · Han-Seok Park* · Hyeong-Beom Park**
(Manuscript=Received FEB 5 ; Revised MAR 14)

Abstract : This paper presents the 3D finite element analysis of the Contact-less Power Supply(CPS) with linear servo motor. The primary, secondary self and leakage inductances of the contact-less power supply and the capacitances of a resonant circuit are calculated by the finite element analysis using current source. The voltage source is used to do accurate analysis of the characteristics of the contact-less power supply. The CPS with the linear servo motor is proposed. The characteristics analysis of the contact-less power supply considering the linear servo motor is done.

Key words : Contact-less power supply, Leakage inductance, Linear servo motor, Resonant circuit.

I. Introduction

In the last ten years, a new energy transmission system, Contact-less Power Supply(CPS), has been developed and now thousands of these kinds of devices using this technology are working in various fields such as underwater vehicle, moving robot and electric vehicle[1]-[5]. The transformer used in the CPS stretches the primary winding into a long loop and places the secondary winding on an open-end core with surrounds the primary conductors and allows relative movement between the two. The reduced coupling of the open core geometry is compensated by a higher primary frequency. So the CPS electric circuit has a high frequency intermediate circuit. There are a few papers dealing with the finite element method (FEM) in modeling the CPS electric circuit. The papers dealing with the finite element method (FEM) in modeling the CPS's electric circuit have not been reported.

This paper presents the 3D finite element analysis of CPS with linear servo motor. The primary, secondary self and leakage inductances are obtained by the 3D finite element analysis using current source and the magnetic coupling coefficients are calculated from these values and compared. The voltage source is used to do accurate analysis of the

† Kyung-il Woo(Pukyong University, Electrical Engineering),E-mail:cogging@pknu.ac.kr, Tel: 051)620-1427
* Pukyong University, Electrical Engineering
** Pukyong University, Electrical Engineering

characteristic of CPS. The CPS with the linear servo motor is proposed. The 3D finite element analysis of CPS considering the linear servo motor is performed.

Ⅱ. Characteristics Analysis

A. Analysis Model

Fig. 1 shows a CPS model with an alternative switching for the primary source adopted in this paper. There are one primary core and two secondary cores. Each secondary core can be used as CPS, that is, there are left and right CPS. The lamination depths of the primary and the secondary core are 300[mm] and 60[mm], respectively. The air gap length is 0.5 [mm] and the frequency is 1000 [Hz]. Turn of coil of the primary is 45 and the secondary is 100. The material type of the primary and secondary core is S45C. The side A of the primary coil and core are segmented to reduce the leakage flux. In this figure, the dotted square box is the secondary core. Fig. 2 shows the 3D structure of side A of CPS.

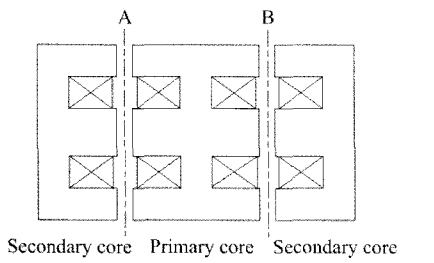

(a) Front view

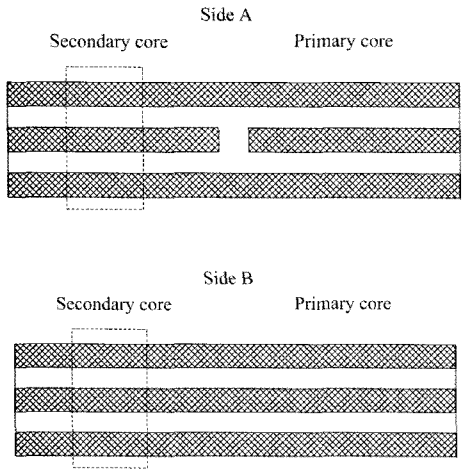

(b) Side view

Fig. 1 Analysis model

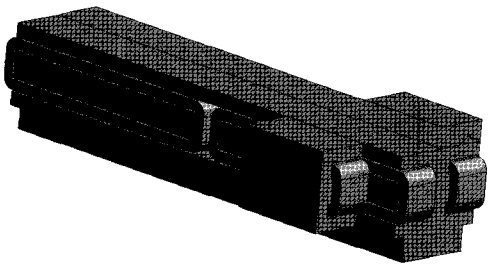

Fig. 2 3D structure of CPS

B. Governing Equation

The fundamental equation of the magnetic field using 3D FEM with edge element can be written using the magnetic vector potential as follows:

$$rot(\nu\, rotA) = J_0 + J_e \tag{1}$$

where ν is the reluctivity, J_0 is the current density and J_e is the eddy current density. J_e is given as follows:

$$J_e = -\sigma(\frac{\partial A}{\partial t} + \nabla\Phi) \tag{2}$$

where σ is the electrical conductivity and Φ is the electric scalar potential.

From (2) and $J_e = 0$, we can obtain the following equation.

$$\nabla \cdot \left\{ -\sigma \left(\frac{\partial A}{\partial t} + \nabla \Phi \right) \right\} = 0 \tag{3}$$

The magnetic field can be calculated by coupling (1)-(3).

The following equations can be obtained by the Galerkin's method from (1) and (3).

$$\begin{aligned} G_i = & \int_V rot\, N_i \cdot (\nu\, rot A) dV - \int_{V_e} N_i \cdot J_0\, dV \\ & + \int_{V_e} N_i \cdot \left\{ \sigma \left(\frac{\partial A}{\partial t} + \nabla \Phi \right) \right\} dV \\ & - \int_S N_i \cdot \{ (\nu\, rot A) \times n \} dS = 0 \end{aligned} \tag{4}$$

$$\begin{aligned} G_{di} = & \int_{V_e} \nabla N_i \cdot \sigma \left(\frac{\partial A}{\partial t} + \nabla \Phi \right) dV \\ & + \int_{S_e} N_i \left\{ -\sigma \left(\frac{\partial A}{\partial t} + \nabla \Phi \right) \right\} \cdot \boldsymbol{n}\, dS = 0 \end{aligned} \tag{5}$$

where N_i is the vector interpolation function for A, N_i is the scalar interpolation function for Φ, V is the analyzed region, V_e is the region of the conductor with the eddy current, S and S_e are the boundary of analyzed region and eddy current region, respectively. $\boldsymbol{n}$ is the unit outward normal vector on the surface S and S_e. The 3D region is divided into tetrahedral elements, and the matrix of the FEM is solved by the CG method and Newton-Rahpson iteration technique is used for the non-linear characteristics.

The circuit equations (6) and (7) should be considered to solve (4) and (5).

$$[U] = [R][I] + [L_0]\frac{d}{dt}[I] + [E] \tag{6}$$

$$[E] = \frac{d}{dt}[\lambda_s] \tag{7}$$

where,

$[U] = (U_a)$: phase voltages,

$[I] = (i_a)$: phase currents,

$[R] = (R_a)$: primary winding resistances,

$[L_0] = (L_a)$: end winding leakage inductances,

$[E] = (E_a)$: phase e.m.f.

$[\lambda_s] = (\lambda_a)$: phase flux linkages.

Ⅲ. Analysis Results

A. Inductance profile and magnetic coupling coefficient

3D FEM is used to analyze the characteristic of the CPS. Because in 3D analysis much longer calculation time is needed we divided the analysis model with coarse meshes. Fig. 3 and Fig. 4 show the inductance profile and the magnetic coupling coefficient of two CPS with a variation of the secondary core position. In Fig. 3, the displacement is the distance from the left position of the primary core to the secondary core position. In this figure, self inductance of the secondary coil, mutual inductances of the primary coil by the secondary coil and self inductances of the primary coil are about the same. But a mutual inductance of the primary coil by the secondary coil is increased at 120[mm] because two primary coils are excited in Fig. 3 (a). At middle position, mutual inductances of the secondary coil by the primary coil are

greater than those of the other position in Fig. 3 (a), (b). The fluctuation of mutual inductance of the secondary coil of the primary coil of Fig. 3 (a) is greater than that of Fig. 3 (b) because the relative length of the primary coil to the secondary coil of left CPS is shorter than that of right CPS. Fig. 4 shows the characteristics of the magnetic coupling coefficient calculated by (8) of two CPS.

$$k = \sqrt{\frac{L_{12}L_{21}}{L_{11}L_{22}}} \tag{8}$$

where L_{12}, L_{21} are mutual inductances, L_{11}, L_{22} are the self inductance of the primary and secondary coil, respectively. It is shown that the magnetic coupling coefficient of the left CPS is better than that of right side because of the leakage inductance but there is a large fluctuation. The fluctuation of magnetic coupling coefficient of left CPS is greater than that of right CPS. The magnetic coupling coefficient of left CPS at 120[mm] is smaller than that of the other positions because of the leakage inductance. Fig. 5 (a) and (b) show the flux plots of CPS when the secondary core is located at 60[mm] and 120[mm]. In Fig. 5 (a), it is shown that there is a lot of leakage flux in right CPS because the length of primary coil is very long. In Fig. 5 (b), because two primary coils are excited lots of leakage flux generated in left CPS. Fig. 6 shows the photo of the manufactured CPS.

B. Electrical scheme of CPS

Fig. 7 shows the electrical scheme of CPS to check the effectiveness of the resonant capacitor. In this figure, the primary series capacitor has been introduced to compensate the very high leakage inductance of the primary and the secondary coils. It is possible to calculate this capacitor from the condition of running at resonance by (9).

$$C_p = 1/\left(4\pi^2 f^2\left(L_{1s} + L_{2s}'\right)\right) \tag{9}$$

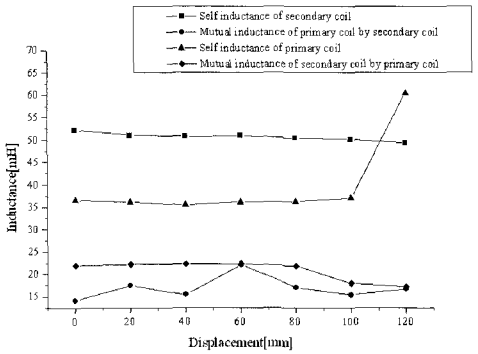

(a) Left CPS

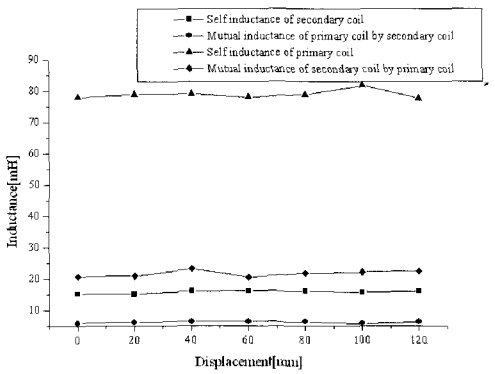

(b) Right CPS

Fig. 3 Inductance profile of CPS

where L_{1s} is the leakage inductance of the primary, L_{2s}' is the referred secondary leakage inductance to the primary. The

secondary parallel capacitor, mounted in the secondary side, compensates the magnetizing inductance. Its value can be also calculated from resonant condition of secondary circuit by (10).

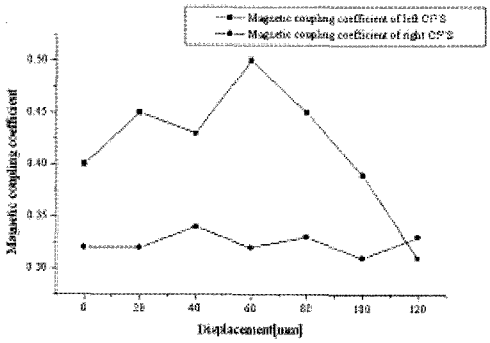

Fig. 4 Magnetic coupling coefficient of CPS

$$C_s = 1/\left(4\pi^2 f^2 L_m''\right) \tag{10}$$

where L_m'' is the referred magnetizing inductance to the secondary.

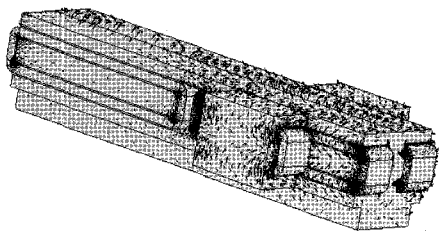

(a) Secondary core is located at 60[mm]

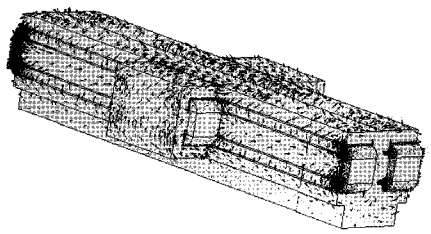

(b) Secondary core is located at 120[mm]

Fig. 5 Flux plots of CPS

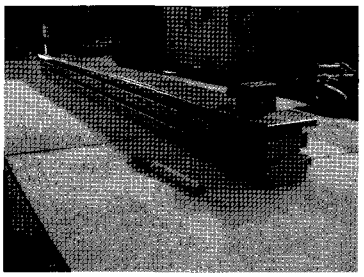

(a) Primary core

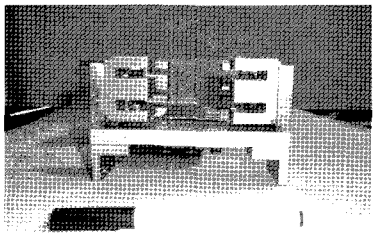

(b) Secondary core

Fig. 6 Photo of CPS

Fig. 8 shows the response of flux linkage of the coils when the resonant capacitor is used or not. The left CPS is analyzed conveniently because the left and right CPS are symmetrical. The response is shown in Fig. 8 (a) when the resonant capacitor is not considered while in Fig. 8 (b) when it is considered. It is shown that the resonant circuit is essential in the driving circuit of CPS.

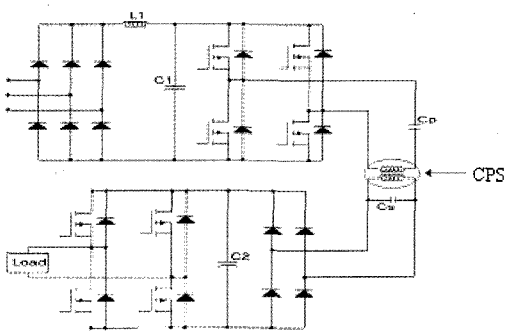

Fig. 7 Electric scheme of CPS

C. CPS with the linear servo motor

Fig. 9 shows the CPS with the linear servo motor. The phase of the motor is 3 and the air gap length is 2[mm]. The core thickness and the core height are 50[mm] and 65[mm], respectively. From this figure, it is known that the directions of the coil current of the CPS and linear servo motor are different. Therefore the 3D finite element analysis is necessary. The 3 phase power obtained from CPS could be inputted to the linear servo motor. The driving circuit of this system is similar to Fig. 7. Because the electric scheme of Fig. 7 is 1 phase circuit it should be corrected to obtain the 3 phase power. Fig. 10 shows the magnetic flux plot when the linear servo motor is excited

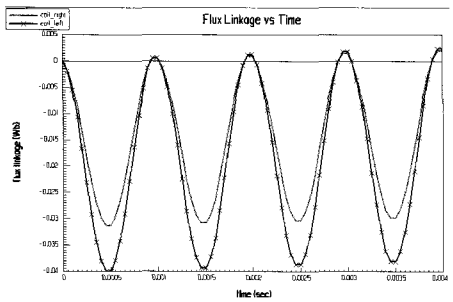

(a) Resonant capacitor is not considered

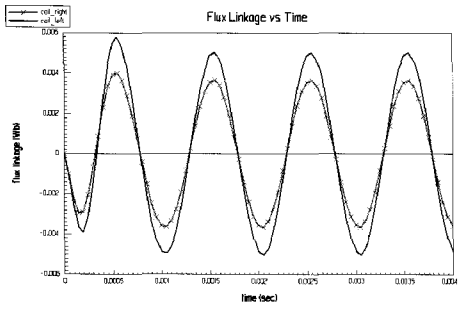

(b) Resonant capacitor is considered

Fig. 8 Flux linkage response

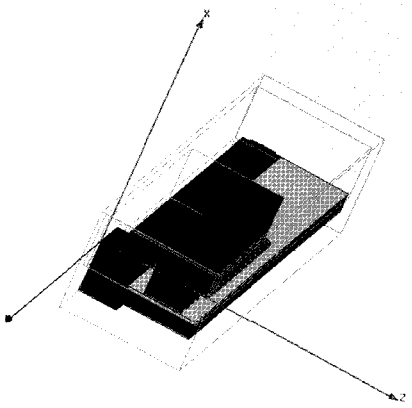

Fig. 9 CPS with linear servo motor

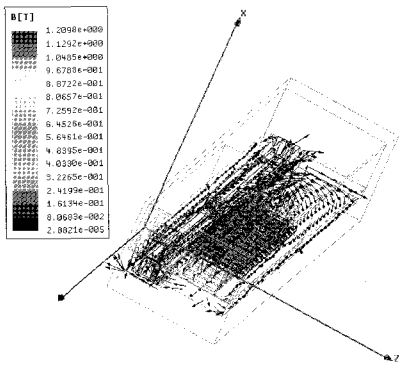

Fig. 10 Magnetic flux plot

by 220V/60Hz. From this figure it is shown that the magnetic flux passes through the primary core. Because the magnetic flux can affect the characteristics of CPS the distance between CPS and the linear servo motor should be considered carefully.

Ⅳ. Conclusions

This paper presents the 3D finite element analysis of CPS with linear servo motor. The primary, secondary self and leakage inductances are obtained by the 3D finite element analysis using current source and the magnetic coupling

coefficients are calculated from these values and compared. The magnetic coupling coefficient of left CPS is greater than that of right CPS. But it is known that driving the left CPS may be difficulty because the capacitance value is fluctuated. We known that the secondary current of left CPS at 60[mm] is greater than that of 120[mm] because of the leakage inductance. The CPS with linear servo motor is proposed. It is shown from the analysis result that the linear servo motor should be located at the proper position not to affect the characteristics of CPS. As a result, we know that the combination of 3D FEM modeling with circuit analysis is useful to obtain a higher modeling accuracy.

Acknowledgment

This work was supported by the Korea Research Foundation Grant. (M01-2004-000- 20380-0)

References

[1] F. Sato, J. Murakami, T. Suzuki, H. Matsuki and S. Kikuchi, "CONTACTLESS ENERGY TRANSMISSION TO MOBILE LOADS BY CLIPS", *IEEE Transaction on Magnetics*, Vol. 33, No. 5, pp. 4203-4205, September 1997.

[2] Shin-ichi Adachi, Fumihiro Sato and Shinki Kikuchi, "Consideration of Contactless Power Station with Selective Excitation to Moving Robot", *IEEE Trans.on Magnetics*, Vol. 35, No. 5, pp. 3583-3585, September 1999.

[3] Tomohiro Kojiya, Fumihiro Sato, Hidetishi Matsuki and Tadakuni Sato, "Construction of Non-contacting Power Feeding System to Underwater Vehicle Utilizing Electro Magnetic Induction", Ocean-Europe, pp. 709-712, 2005.

[4] Y. Kanai, M. Mino, T. Sakai and T. Yachi, "A Non-Contact Power Supply Card Powered by Solar Cells for Mobile Communications ", *IEEE APEC Record*, pp. 1157-1162, 2000.

[5] A. Ghahary and B. H. Cho, "Design of Transcutaneous Energy Transmission System Using A Series Resonant Converter", *IEEE Power Electronics Specialist's Conf. Record*, pp.1-8, 1990.

저 자 소 개

Kyung il Woo

He received the B.S, M.S., and Ph. D. degrees in Electrical Engineering from Hanyang University. He is currently a assistant professor in the Division of Electrical Control Engineering of Pukyong National University.

Han Seok Park

He received the B.S. and M.S. degrees in Electrical Engineering from Jung Ang University. He received the Ph.D. degree in Electrical Engineering from Korea Maritime College. He is currently a professor in the Division of Electrical Control Engineering of Pukyong National University.

Hyeong Beom Park

He received B.S. and M.S. degrees in Electrical Engineering from Pukyong National University. He is currently in the Ph.D. course in Electrical Engineering from Pukyong National University.